

RESEARCH

Open Access



Berberine-loaded PLGA nanoparticles alleviate ulcerative colitis by targeting IL-6/IL-6R axis

Chao Liu¹, Qiming Gong^{1,2,3}, Wanning Liu^{2,3,4}, Yihan Zhao^{2,3,5}, Xinhao Yan^{6*} and Tao Yang^{7,8*}

Abstract

Aims The present study aims to develop a nano-delivery system that encapsulates berberine (BBR) into PLGA-based nanoparticles (BPL-NPs), to treat ulcerative colitis (UC). Furthermore, the therapeutic efficacy and molecular targeting mechanisms of BPL-NPs in the management of UC are thoroughly examined.

Methods Emulsion solvent-driven methods were used to self-assemble BBR and PLGA into nanoparticles, resulting in the development of the nano-delivery system (BPL-NPs). The therapeutic effectiveness of BPL-NPs was evaluated using a dextran sulfate sodium (DSS)-induced model of ulcerative colitis in mice and a lipopolysaccharide (LPS)-induced model of inflammation in THP-1 macrophages. The interaction between M ϕ s and NCM-460 cells was investigated using a co-culture system. The molecular targeting ability of BPL-NPs in the treatment of UC was validated through in vitro as well as in vivo experiments.

Results The BPL-NPs demonstrated a particle size of 184 ± 22.4 nm, enhanced dispersibility in deionized water, and a notable encapsulation efficiency of $31.1 \pm 0.2\%$. The use of BPL-NPs clearly improved the clinical symptoms and pathological changes associated with UC in mice while also ensuring minimal toxicity. In addition, BPL-NPs improved intestinal epithelial cell apoptosis and enhanced the function of the intestinal barrier by inhibiting M1 M ϕ s infiltration and IL-6 signaling pathway in mice with UC. Furthermore, the BPL-NPs were found to selectively target the IL-6/IL-6R axis during the M1 M ϕ s-induced apoptosis of NCM460 cells.

Conclusion The BPL-NPs were confirmed to harbor anti-inflammatory effects both in vitro and in vivo, along with enhanced water solubility and bioactivity. In addition, the precise targeting of the IL-6/IL-6R axis was confirmed as the mechanism by which the BPL-NPs exerted therapeutic effects in UC, as demonstrated in both in vitro as well as in vivo studies.

*Correspondence:

Xinhao Yan

xhyan82@163.com

Tao Yang

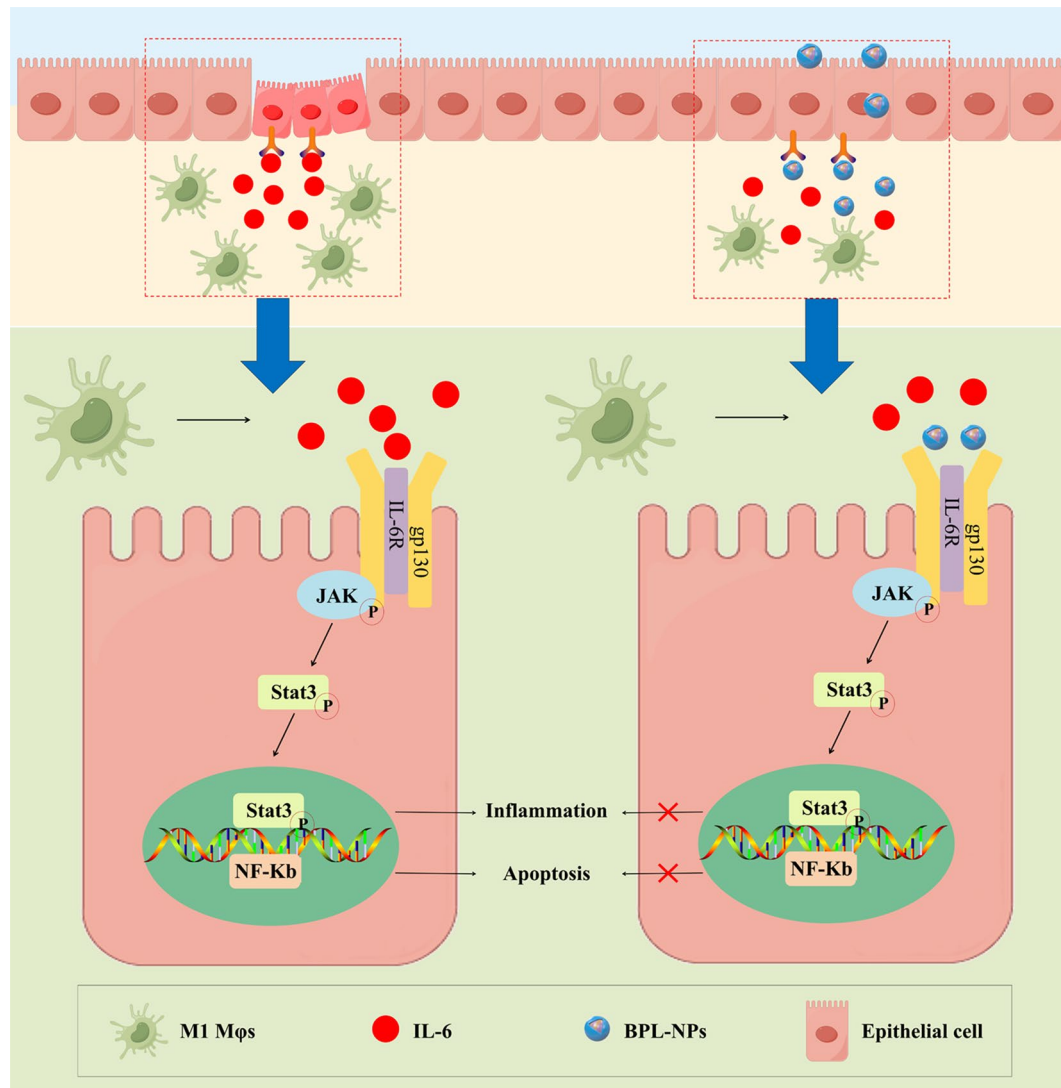
yangtao901212@163.com

Full list of author information is available at the end of the article



© The Author(s) 2024. **Open Access** This article is licensed under a Creative Commons Attribution-NonCommercial-NoDerivatives 4.0 International License, which permits any non-commercial use, sharing, distribution and reproduction in any medium or format, as long as you give appropriate credit to the original author(s) and the source, provide a link to the Creative Commons licence, and indicate if you modified the licensed material. You do not have permission under this licence to share adapted material derived from this article or parts of it. The images or other third party material in this article are included in the article's Creative Commons licence, unless indicated otherwise in a credit line to the material. If material is not included in the article's Creative Commons licence and your intended use is not permitted by statutory regulation or exceeds the permitted use, you will need to obtain permission directly from the copyright holder. To view a copy of this licence, visit <http://creativecommons.org/licenses/by-nc-nd/4.0/>.

Graphical Abstract



Keywords Ulcerative colitis, Berberine, Nanoparticles, IL-6/IL-6R axis

Introduction

Ulcerative colitis (UC) is a chronic immune-mediated disease characterized by recurring and remitting inflammation of the rectum's mucosal lining, which may also extend to the colon's proximal segments. The incidence of UC, as well as the rate of mortality caused by UC has been increasing each year in industrialized nations, particularly in Europe and North America [1]. At present, the management of UC typically commences with drug therapy, including the administering of 5-aminosalicylate acid, corticosteroids, antibiotics, or anti-tumor necrosis factor therapies [2, 3]. However, at the end of treatment, only 40% of patients experience clinical remission while also experiencing various side effects such as moon face,

osteoporosis, type 2 diabetes mellitus, depression, and cataracts [4]. Accordingly, these limitations necessitate the investigation of novel drugs to effectively treat UC.

There has been evidence that traditionally Chinese medicine (TCM) compounds can inhibit chronic and acute intestinal inflammation [5]. Furthermore, they can also regulate the composition of intestinal flora and enhance the function of the intestinal epithelial barrier [6]. Nonetheless, most natural compounds exhibit low water solubility, reduced bioavailability and chemical stability, and are rapidly metabolized in vivo [7–9]. Berberine (BBR), which forms a critical component of TCM, is a natural isoquinoline alkaloid found in plants such as *Berberis vulgaris*, *Cortex phellode*, and *Rhizoma*

coptidis. BBR has been extensively used in medical settings for anti-inflammatory, anticancer, antidiabetic, and possesses high-affinity protein targets (including ROCK2, PIK3CD, KCNMA1, CSF1R and KIT) [10]. It has been demonstrated that BBR was able to improve macrophage M2 polarisation in UC [11]. In addition, BBR has been demonstrated to effectively treat UC by suppressing immune-inflammatory responses and regulating metabolic homeostasis in the host [12, 13]. Accordingly, BBR has been demonstrated to significantly reduce inflammation caused by DSS-induced UC. However, BBR has low water solubility and limited bioavailability. Furthermore, it has a short half-life, and can result in side effects caused by systemic exposure or non-specific biodistribution following oral or parenteral administration. Consequently, the use application of BBR in clinical settings is limited. Thus, the use of BBR encapsulation strategies, which facilitates the development of novel drug delivery systems that retain the efficacy and targeting abilities of BBR, offers significant promise in addressing these limitations.

The advent of nanomedicine in recent years has provided novel insights into innovative therapeutic strategies, effectively transforming the treatment of UC. Nano-delivery systems can be designed to enhance the solubility and stability of drugs, improve their bioavailability, regulate their release rate, increase the concentration of the drug at the desired site, and reduce the systemic toxicity of therapeutic drugs [14]. In this context, nanoparticles (NPs) composed of gelatin, cellulose, and chitosan have been utilized for the targeted delivery of anti-inflammatory drugs to inflamed colonic tissue, resulting in improved therapeutic outcomes in UC [15–17]. Furthermore, previous studies have utilized the cell membrane as a carrier to deliver a wide range of drugs, including BBR, to specifically target inflamed colonic tissue and immune cells [18, 19]. However, the fabrication of cell membrane-encapsulated nanobionic drug delivery systems is complex and difficult to regulate. The typical size of a cell ranges from 5 to 100 μm ; thus, it needs to be significantly reduced for use as a nanoscale delivery system. Poly (lactide-co-glycolide) (PLGA) has been approved as a pharmaceutical excipient by the Food and Drug Administration. It exhibits high biocompatibility and has been frequently used as a delivery vehicle for therapeutic substances [20]. In addition, PLGA-based NPs have been used to deliver BBR in treating cardiovascular disease and tumors, resulting in improved therapeutic outcomes [21, 22].

The present study involved the development of a nano-delivery system with anti-inflammatory properties. The system was created using BBR and PLGA-based NPs through a process called emulsion solvent-driven self-assembly. Consequently, it was theorized that by

enclosing BBR within PLGA and incorporating it into NPs, the therapeutic efficacy in UC could be enhanced. Accordingly, experiments were investigated in vitro as well as in vivo to determine the mechanisms that explain the therapeutic effects of this BBR-encapsulated nanotherapy.

Materials and methods

Reagents and drugs

Detailed information on the reagents and drugs used in this study can be found in Table S1.

Preparation of berberine-loading PLGA nanoparticles (BPL-NPs)

For the emulsion solvent evaporation fabrication, 5 mg PLGA with varying concentrations of BBR (ranging from 0 to 2 mg) were mixed in 1 mL of dichloromethane to form an oil phase. Then, 6 mL of deionized water containing 1.2 mg Lecithin was added to this oil phase. Subsequently, emulsification was carried out using a probe sonicator, with a duration of 3 min and a power level of approximately 150 W. Oil-in-water nanoemulsions are evaporated using a rotary evaporator at ambient temperature to remove solvents. Correspondingly, the resulting mixture was then dialyzed for 24 h in deionized water, after which it was lyophilized. A BBR-PLGA formulation incorporating Cyanine 5 (Cy 5) was prepared using a similar approach. 0.5 mg of Cy 5 NHS ester, 1 mg of BBR, and 5 mg of PLGA were dissolved in 1.5 mL of dichloromethane to prepare the oil phase.

A 450 nm microplate reader (Epoch, BioTek, USA) was used to measure BBR concentration in BBR-PLGA. Following are the equations used to determine drug loading content and entrapment efficiency.

$$\begin{aligned} \text{Drug loading content (\%)} \\ &= \text{Weight of BBR in NPs} / \text{Weight of BBR-loaded NPs} \times 100\% \end{aligned}$$

$$\begin{aligned} \text{Entrapment efficiency (\%)} \\ &= \text{BBR content in NPs (\%)} / \text{Theoretical BBR content (\%)} \times 100\% \end{aligned}$$

Bioinformatics and immune infiltration analysis of UC

RNA expression arrays of UC patients were obtained using the Gene Expression Omnibus (<http://www.ncbi.nlm.nih.gov/geo>). An empirical Bayesian approach was used to identify differentially expressed genes (DEGs) using the Bioconductor “Limma” package within the R environment. There were significantly up-regulated and down-regulated DEGs with a logFC (fold change) greater than or equal to 1.0 and a false discovery rate of 0.05 or less. Subsequently, in order to investigate the differences in gene expression between two distinct sets of phenotypic samples, GSEA was used. Gene sets with a

normalized enrichment score (NES) ≥ 1.5 or -1.5 , and an adjusted P -value (P_{adj}) ≤ 0.05 , were deemed to be significant. In addition, the CIBERSORT deconvolution algorithm was utilized to examine the immune infiltration of both the UC and healthy samples, using gene expression profiles. The permutation (perm) was adjusted to 1000 to achieve more excellent result stability. In addition, we also measured the enrichment scores of macrophages, B cells, CD8+T cells, DCs, neutrophils, and natural killer cells using single sample gene set enrichment analysis (ssGSEA). Furthermore, the enrichment scores of immune functions such as antigen-presenting cell (APC) co-inhibition, chemokine receptors (CCR), human leukocyte antigen (HLA), parainflammation, T cell co-inhibition, and T cell co-stimulation were also quantified. P -value < 0.05 was used to filter the samples. In addition, the correlation between the expression of hub genes and the presence of immune-infiltrated cells, as analyzed by CIBERSORT, was assessed using the Pearson correlation coefficient ($P < 0.05$).

Design of animal experiments

The use of the animal model involving male mice with induced UC using a 3% DSS (w/v) solution was reported previously in earlier studies [11–13]. The mice used in the experiments were randomly assigned to one of four groups: control, UC, PLGA-NPs, and BPL-NPs. Each group constituted a combined total of 10 mice. The study employed a retention enema to administer the NPs. Accordingly, the control and UC mice were given a 0.2 ml dose of 0.9% N.S for 7 days. Subsequently, each group received 0.2 ml of PLGA-NPs and 0.2 ml of BPL-NPs (with a concentration of 0.09 mg/mL), respectively. Finally, the colon tissue samples were obtained from all mice, following their euthanasia, stored at a temperature of -80 , and subsequently utilized for additional experiments. All experimental procedures were approved by the Fourth Military Medical University's Ethics Committee in accordance with the National Institutes of Health Guide for the Care and Use of Laboratory Animals.

Disease performance and disease activity index (DAI)

The severity of UC was assessed by daily monitoring of disease activity, which included tracking body weight, stool consistency, and fecal occult blood. The DAI score was calculated using the scoring system outlined by Wirtz et al. [23]. The system includes a weight loss score, a diarrhea score, and an occult blood score. On Day 14, the experiment concluded and all mice were euthanized. Subsequently, the colon tissues were collected.

Identification of M1 M ϕ in the colon and immunofluorescence (IF) staining

The colon tissue was stained using the immunofluorescence (IF) protocol described by Im et al. [24]. The fluorescent markers used to identify the M1 M ϕ in the intestine comprised F4/80⁺ CD86⁺ (1:50). On the other hand, the colon tissue sections were treated with a polyclonal anti-IL-6 Ab (1:50) and an anti-Caspase-3 Ab (1:50). Subsequently, fluorescent images were acquired via fluorescence microscopy at a magnification of 200X (Olympus, Japan).

Transmission electron microscope (TEM)

The colon samples were preserved using a solution containing 2.5% glutaraldehyde (pH 7.4) and 1% osmium tetroxide. The specimens were desiccated using alcohol and acetone, and then encased in araldite. Subsequently, the tissues were cut into slices measuring 60–70 nm thick. These slices were then treated with uranyl acetate and lead citrate for staining. Subsequently, the ultrastructure of the intestinal mucosa and tight junction complexes in colon tissues were examined and photographed.

Cell culture and co-culture system

Both THP-1 (ATCC, USA) and NCM-460 (normal colonic epithelial cells) (Fenghui Biological Cell Center) cell lines were used in this study. A humidified environment containing 5% CO₂ and 10% fetal bovine serum was used to cultivate the two cell lines in RPMI-1640 medium supplemented with 1% penicillin/streptomycin at 37 °C. The THP-1 cells were cultured in a 6-well plate with a density of 1.5×10^6 cells per well. They were then exposed to 10 ng/mL of PMA and 0.3% bovine serum albumin for 48 h. After THP-1 cells were confirmed to be M ϕ s, LPS (200 ng/mL) was administered to generate M1-polarized M ϕ s. The characteristics of NCM-460 cells were examined by co-culturing M ϕ s derived from THP-1 cells and NCM-460 cells. The NCM-460 cells were cultured in a 6-well plate with a density of 2×10^5 cells per well for 12 h, and then transferred to the lower transwell chamber. The induced M ϕ s were subsequently introduced into the upper chamber at a density of 1.5×10^6 cells/well. The duration of the co-cultivation system ranged from 24 to 48 h.

Flow cytometry (FCM) analysis

Flow Cytometry (FCM) was utilized to analyze the process of apoptosis in NCM460 cells and to detect the fluorescence of Cy5. The Apoptosis Detection Kit was acquired from BD (San Jose, CA). NCM460 cells were harvested and subsequently labeled with Annexin V/PE and 7-amino-actinomycin (7-AAD) in a 400 μ l binding buffer solution. The cells were cultured for 20 min at

ambient temperature, and the apoptosis rate was analyzed using FCM (BD, FACSCanto II, USA).

High-content system (HCS) array

The HCS array system was utilized for the morphological identification of NCM460 cells. Accordingly, fluorescent dyes, including Hoechst 33,342, ethidium homodimer-1 (EthD-1), and Calcein AM, which have been reported previously, were used in the current study [25]. The configuration of the HCS array system adhered precisely to the guidelines outlined in the instruction manual.

siRNA transfection

The IL-6R knockdown assay involved using IL-6R-targeting small interfering RNAs (siRNAs) prepared by GenePharma Ltd (Shanghai, China). Following specific instructions, these siRNAs were cloned into NCM460 cells using JET (jetPRIME). Non-homologous scrambled sequences were used as negative controls (NC). The efficacy of knockdown was confirmed through RT-qPCR (Fig. S1).

RNA sequencing and gene set enrichment analysis

In order to assess the alterations in the transcriptome of colonic tissues among various groups, colonic tissues were collected and total RNA was isolated using the TRIzol method. RNA-seq transcriptome library was generated using the Illumina® Stranded mRNA Prep, Ligation kit from Illumina (San Diego, CA) using 1 µg of total RNA. The differential expression genes (DEGs) were determined using the transcripts per million reads (TPM) method and analyzed using the DESeq2 software. Accordingly, DEGs with $|\log_2FC| \geq 1.0$ or -1.0 and P value < 0.05 were considered significant DEGs.

PCR array and qRT-PCR

Total RNA was extracted from colon samples or NCM460 cells using TRIzol, and the cDNA was then reversed using the PrimeScript RT Reagent Kit, following the manufacturer's protocol. The cDNA was analyzed using PCR Array (Wcgene Biotech, Shanghai, China) to detect the expression of all mRNA in the pathway. Accordingly, quantitative real-time PCR (qRT-PCR) was performed in triplicates using the CFX Connect Real-Time PCR System (BIO-RAD). GAPDH functioned as an internal reference gene. The primers are displayed in Table S1.

Western blot analysis

Protease inhibitors in the Radio-Immunoprecipitation Assay (RIPA) buffer were used to collect total protein from colon samples. The total protein sample was subjected to electrophoresis using 10% SDS polyacrylamide gels and transferred to PVDF membranes. The

membranes were immersed in a solution of 5% fat-free milk for 2 h, followed by incubation with the specified primary and secondary antibodies. The data about antibodies is presented in Table S1. The gray signal of the blots was detected using an enhanced chemiluminescence (ECL) kit with the e-Blot equipment (e-Blot, Shanghai).

Statistics analysis

The data were reported as the mean \pm standard deviation (SD) and were analyzed using the SPSS software program (version 21.0). Data were presented using one-way ANOVA followed by LSD test. For the data of repeated measurement, repeated measures analysis of variance was applied, and the LSD method was used for multiple comparisons. A significance level of $P < 0.05$ was deemed statistically significant, while a significance level of $P < 0.01$ was considered highly significant. The results were visually presented using R software and GraphPad Prism software.

Results

Characterizations of BPL-NPs

The significant challenges to the widespread application of BBR include its limited water solubility and its reliance on specific organic solvents. In order to address this constraint, BBR-loading PLGA nanoparticles (BPL-NPs) were synthesized (Fig. 1A). BPL-NPs containing BBR were produced using a double emulsion solvent evaporation approach. Initially, we synthesized PLGA-NPs in the presence of lecithin. Consequently, the resulting NPs exhibited a typical core-shell structure, wherein a lecithin shell enveloped a hydrophobic core. In this context, the TEM analysis revealed that the PLGA-NPs had a distinct and clearly defined spherical shape, as depicted in Fig. 1B. Additionally, the dynamic light scattering measurements results indicated that the PLGA-NPs exhibited a narrow size distribution (Fig. 1C), with an average diameter of 162.2 nm and a zeta-potential of -23.4 ± 1.7 mV (Fig. 1D). Subsequently, various BPL-NPs were prepared. BBR was combined with PLGA in a 6:1 ratio in lecithin-free water, using dichloromethane as a solvent. This mixture was subjected to sonication at room temperature for a duration of 3 min. Subsequently, the effects of various concentrations of BBR (ranging from 0.5 to 2 mg) on the mean diameter of the resulting NPs (Fig. 1E) and their polydispersity index (Fig. 1F) were analyzed. Optimal results were obtained when the BBR content was 1.75 mg, as demonstrated by the morphology and distribution of the resulting NPs. TEM observations (Fig. 1G) revealed that the NPs formed by BPL were nearly spherical in shape, with a mean hydrodynamic diameter of 184 ± 22.4 nm, as quantified via dynamic light scattering (Fig. 1H). In addition, the zeta-potential of the as-obtained NPs was

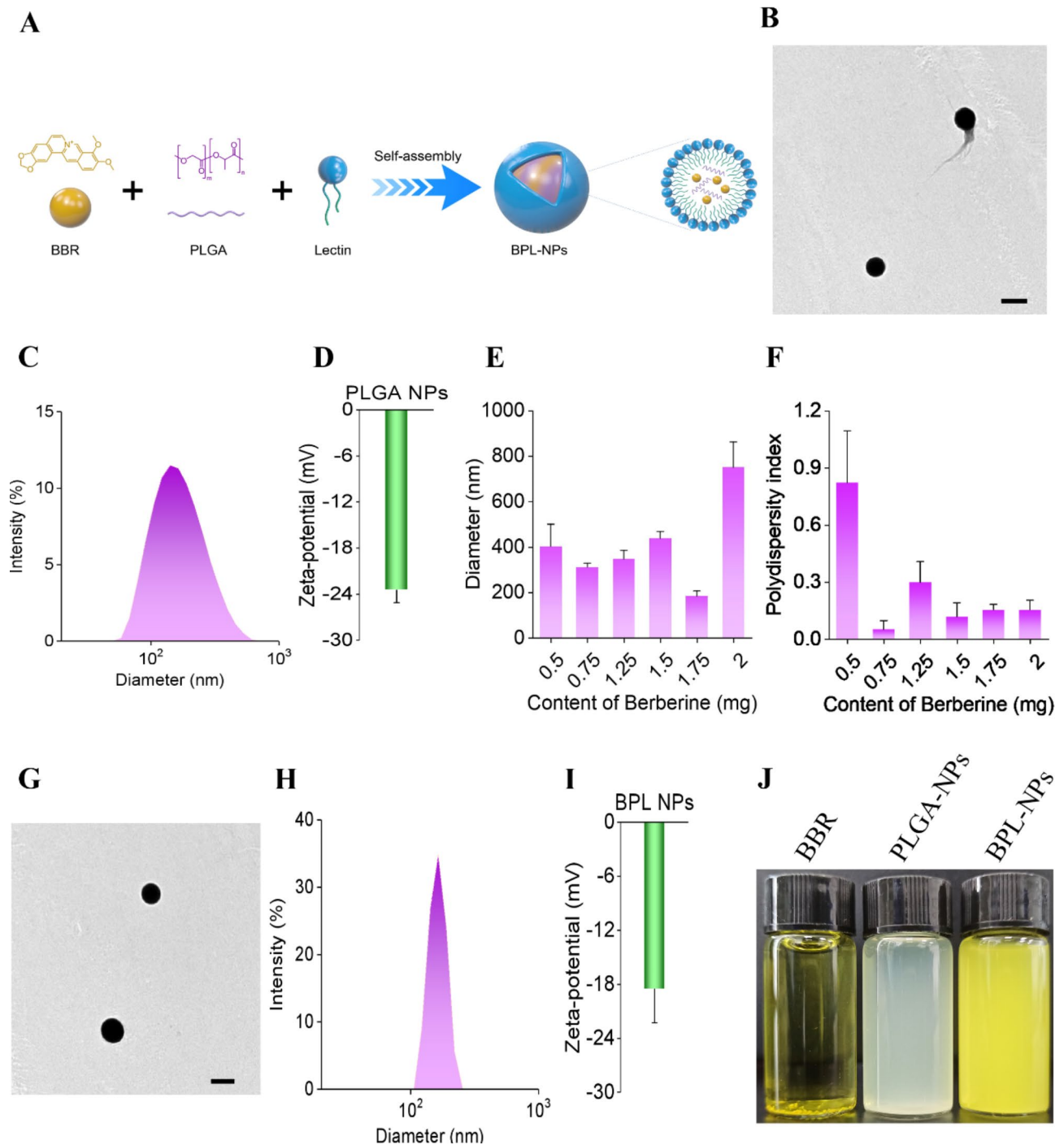


Fig. 1 Fabrication and characterization of BPL-NPs. **A:** Schematic diagram illustrating the fabrication of BPL-NPs using an emulsion solvent evaporation method; **B–D:** TEM (**B**), size distribution (**C**), and zeta-potential (**D**) of PLGA nanoparticles; **E,F:** Mean diameters (**E**) and polydispersity index (**F**) of different BPL-NPs; **G–I:** TEM (**G**), mean diameters (**H**), and zeta-potential (**I**) of BPL-NPs; **J:** Dispersion of BBR, PLGA-NPs, and BPL-NPs. Scale bars = 200 nm

determined to be negative, specifically -18.5 ± 3.8 mV (Fig. 1I). Evidently, BPL-NPs have better dispersibility in deionized water, as shown in Fig. 1J. Furthermore, the polydispersity index was less than 0.2, suggesting a relatively limited range of sizes for the BPL-NPs. In addition, the BBR loading content and entrapment efficiency for

BPL-NPs were $31.1 \pm 0.2\%$ and $54.7 \pm 0.4\%$, respectively, with a concentration of $256.15 \mu\text{M}$ (Table S2).

Cellular uptake of BPL-NPs in vitro

Ensuring the effective internalization of BPL-NPs by cells is a crucial prerequisite for achieving high therapeutic

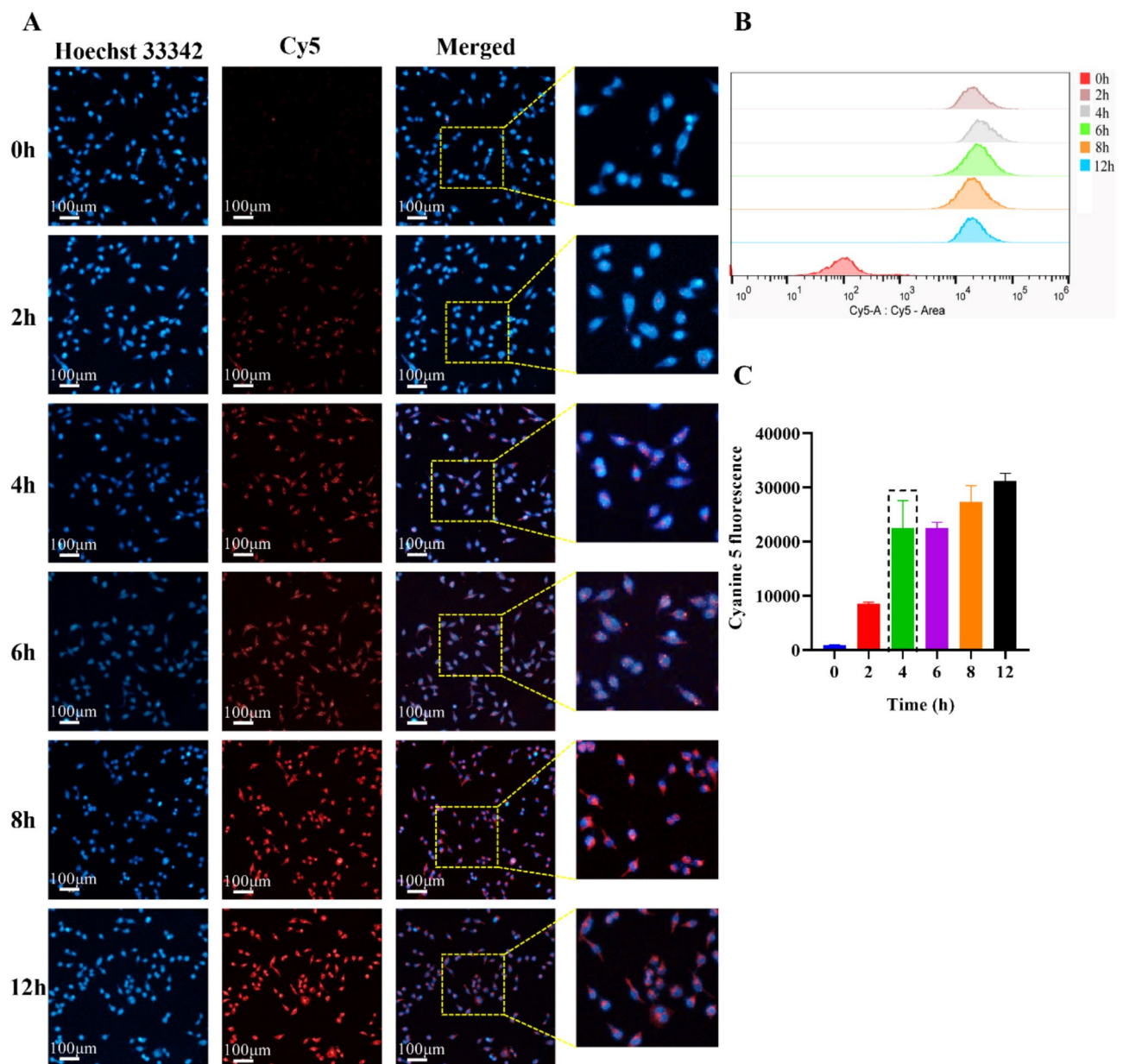


Fig. 2 Measurement of cellular uptake of BPL-NPs in vitro. **A:** HCS images of Cy 5 fluorescence in NCM460 cells; **B:** Kurtogram of Cy 5 detected by FCM at various time intervals; **C:** Quantification of Cy 5 fluorescence detected by FCM at various time intervals

efficacy. To verify the targeting efficacy of BPL-NPs, a cellular uptake experiment was conducted using NCM460 cells. The ideal concentration of BPL-NPs for NCM460 cells was determined to be 20 μ M, resulting in a cell viability of over 90% (92.51 ± 16.02 , Fig. S2). In addition, the HCS array imaging demonstrated intense Cy 5 fluorescence signals, which were localized in the cytoplasm or on the membrane of NCM460 cells following a 4-hour incubation period (Fig. 2A). Furthermore, the fluorescence of Cy 5, as detected by FCM, exhibited a plateau in uptake after 4 h of incubation (Fig. 2B and C). As the duration of time increased, the process of cellular uptake

gradually became more pronounced and peaked at 12 h of incubation (Fig. 2C). These results demonstrate that the BPL-NPs were rapidly internalized into the membrane or cytoplasm of NCM460 cells.

IL-6 signaling pathway promoted the immune-infiltrating of M1 M ϕ s in UC

The GSE87473 database [26], comprising 106 UC patients and 21 healthy individuals, was also analyzed in this study. There were 2805 DEGs identified, of which 468 were upregulated and 523 were downregulated (Fig. 3A). In addition, the GSEA results revealed significant

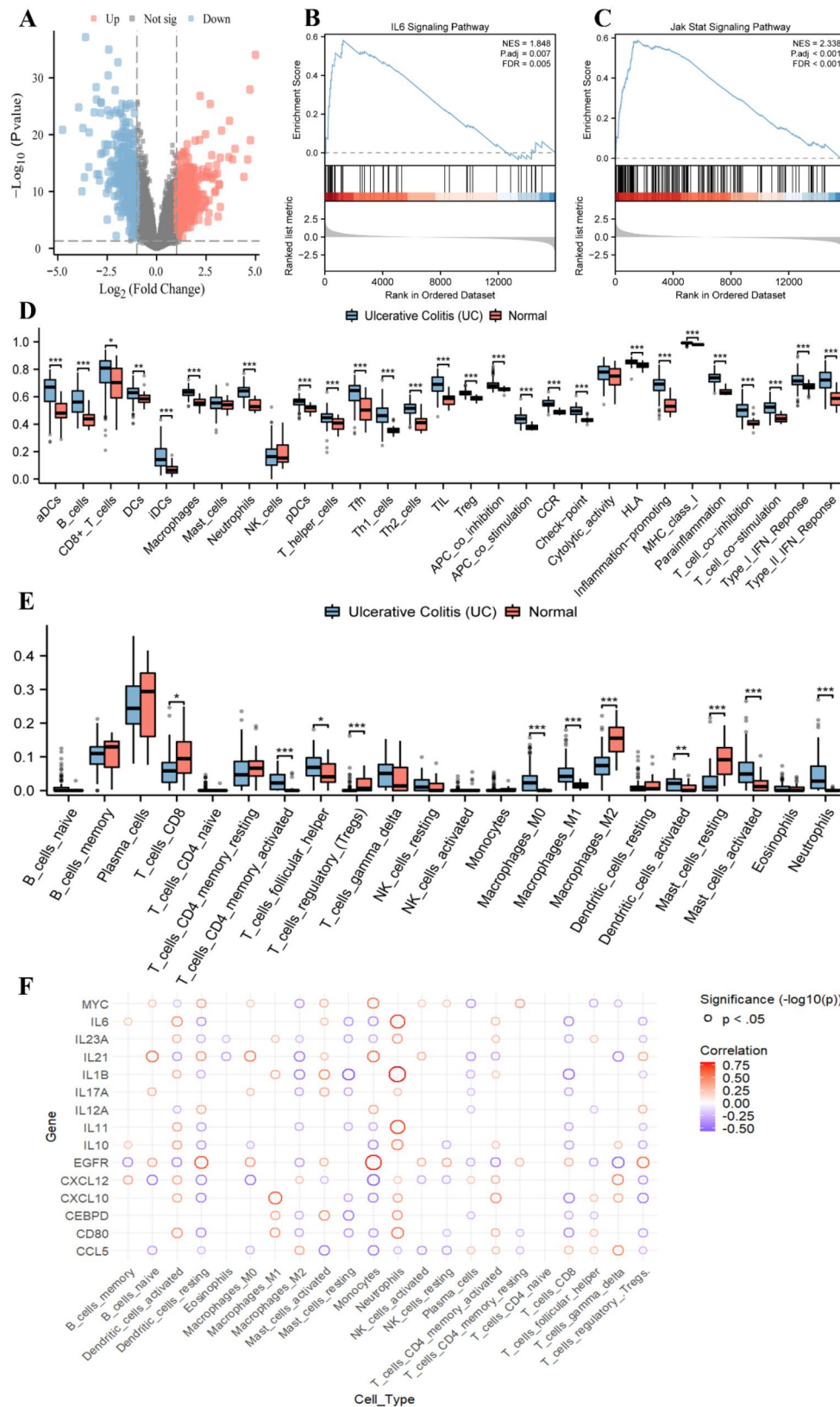


Fig. 3 Bioinformatics and immune infiltration analysis of the UC and healthy groups. **A:** Volcano plot of DEGs in the GSE87473 database; **B:** GSEA of IL-6 signaling pathway in the GSE87473 database; **C:** GSEA of JAK-STAT signaling pathway in the GSE87473 database; **D:** Immune cells infiltration and function analysis between UC and healthy samples; **E:** Subtypes of immune cells infiltration analysis between UC and healthy samples; **F:** Correlation matrix of hub genes in the IL-6 signaling pathway and immune cell subtypes in UC. * $P < 0.05$, ** $P < 0.01$ and *** $P < 0.001$

upregulation of the IL-6 signaling pathway (NES=1.848, $P_{\text{adj}} = 0.007$, Fig. 3B, Table S3) and JAK-STAT signaling pathway (NES=2.338, $P_{\text{adj}} < 0.001$, Fig. 3C, Table S3) in the UC phenotype. Furthermore, these results indicated that the IL-6 and JAK-STAT signaling pathways were over-activated, which was the primary mechanism responsible for UC. Subsequently, both the UC and healthy samples were analyzed for immune infiltration. The differential analysis of immune cells showed that patients with UC exhibited a significantly elevated level of macrophages (M ϕ s), when compared to other groups ($^{***}P < 0.001$, Fig. 3D, Table S4). An analysis of immune function further revealed that UC patients exhibited significant levels of CCR (chemokine receptors), HLA (human leukocyte antigen), inflammation-promoting factors, and parainflammation (Fig. 3D, Table S4). Subsequently, a more in-depth examination of the different categories of immune cells was conducted. The findings revealed a notable increase in M0 and M1 M ϕ s among UC patients. In contrast, the healthy group exhibited significantly higher levels of M2 M ϕ s ($^{***}P < 0.001$, Fig. 3E). In addition, the correlation analysis between hub gene expression in the over-activation IL-6 signaling pathway [27] and immune-infiltrated cells further revealed that the expression of CD80, CEBPD, CXCL10, IL1B, and IL23a was positively correlated with the activation of M1 M ϕ s. Nevertheless, the gene expression in the IL-6 signaling pathway exhibited a negative correlation with M2 M ϕ s, with the exception of CCL5 and CXCL12 (Fig. 3F, Table S5). These findings demonstrate that the activation of the IL-6 signaling pathway significantly enhanced the immune infiltration of M1 M ϕ s in UC, as indicated by the expression of their signatures.

BPL-NPs ameliorated disease performance of UC mice

Current research also investigated the therapeutic effects of BPL-NPs on UC mice induced by DSS. As illustrated in Fig. 4A, in comparison to the control and BPL-NPs groups, the colon length of the UC group was considerably shorter. Colon length increased significantly after administering BPL-NPs. Furthermore, the UC group exhibited noticeable weight loss starting on the fourth day. On the other hand, the weight loss of UC mice in the BPL-NPs group was significantly alleviated (Fig. 4B). In addition, the DAI values exhibited a significant decrease following treatment with BPL-NPs, which can be attributed to alleviating symptoms such as weight loss, diarrhea, and positive results in the fecal occult blood test (Fig. 4C). The H&E staining revealed a predominant infiltration of neutrophils and lymphocytes in the mucosa and lamina propria of the UC group, as shown in Fig. 4D. Conversely, the pathological changes observed in the BPL-NPs group were less pronounced than those observed in the UC group. Moreover, a significant

increase in goblet cells in the crypts of the colon was observed after administration of BPL-NPs, as well as a significant reduction in neutrophil and lymphocyte infiltration (Fig. 4D). These findings clearly demonstrate that the BPL-NPs possess the required attributes to effectively treat UC.

BPL-NPs ameliorated apoptosis of intestinal epithelial cells via inhibiting M1 M ϕ s in UC mice

Previous results, as shown in Fig. 3E and F, revealed a notable increase in the presence of M1 macrophages and the expression of IL-6 in UC patients. As a result, triple-labeling markers (F4/80 $^{+}$ CD86 $^{+}$ IL6 $^{+}$) were used to identify M1 M ϕ s in the colon specifically. As anticipated, the colon lining of the UC mice was significantly infiltrated with M1 M ϕ s (CD86 $^{+}$, indicated by green fluorescence) (Fig. 5A). In addition, the expression of IL-6 $^{+}$ (indicated by yellow fluorescence) was considerably higher in the colon mucosa (Fig. S3). However, following treatment with BPL-NPs, there was a notable reduction in the proportion of infiltrated M1 M ϕ s and the expression of IL-6 $^{+}$ in the intestinal mucosa (Fig. 5A). Subsequently, an assessment of intestinal epithelial cell (IECs) apoptosis and mucosal barrier integrity was carried out using BPL-NPs. As shown in Fig. 5B and S4, the use of BPL-NPs significantly reduced the apoptosis ratio of IECs, as indicated by the results of the TUNEL analysis. Consistent with the above, Caspase-3, an activated apoptosis marker, was also decreased by the treatment of BPL-NPs (Fig. 5C, Fig. S5). In addition, the TEM results indicated that treatment with BPL-NPs effectively reduced the disruption of the intestinal barrier and tight junctions caused by DSS, as demonstrated in Fig. 5D. Owing to the fact that an endemic route of administration was adopted in this study, no discernible toxic effects were found on major organs such as the heart, liver, spleen, lungs, and kidneys (Fig. 5E). Based on these results, BPL-NPs were found to reduce apoptosis of IECs, inhibit M1 macrophage infiltration, and inhibit IL-6 expression in mice with UC.

BPL-NPs down-regulated inflammatory response pathways in UC mice

The transcriptomics analysis revealed a total of 5,887 DEGs in the UC group, when compared to the control group (Fig. 6A, Table S6). Among these DEGs, 3,157 were upregulated and 2,730 were downregulated. In this context, the transcriptional expression level of Il-6 (Fig. 6B) and its membrane receptor, Il-6R α (Fig. 6C), were found to be significantly upregulated in the UC group. Furthermore, the results of GSEA indicated that the inflammatory response pathway (Fig. 6D, Table S7) was significantly upregulated in the UC phenotype. In addition, all inflammatory pathways, such as interleukin 6 family signaling (Fig. 6E), Il6 signaling pathway (Fig. 6F),

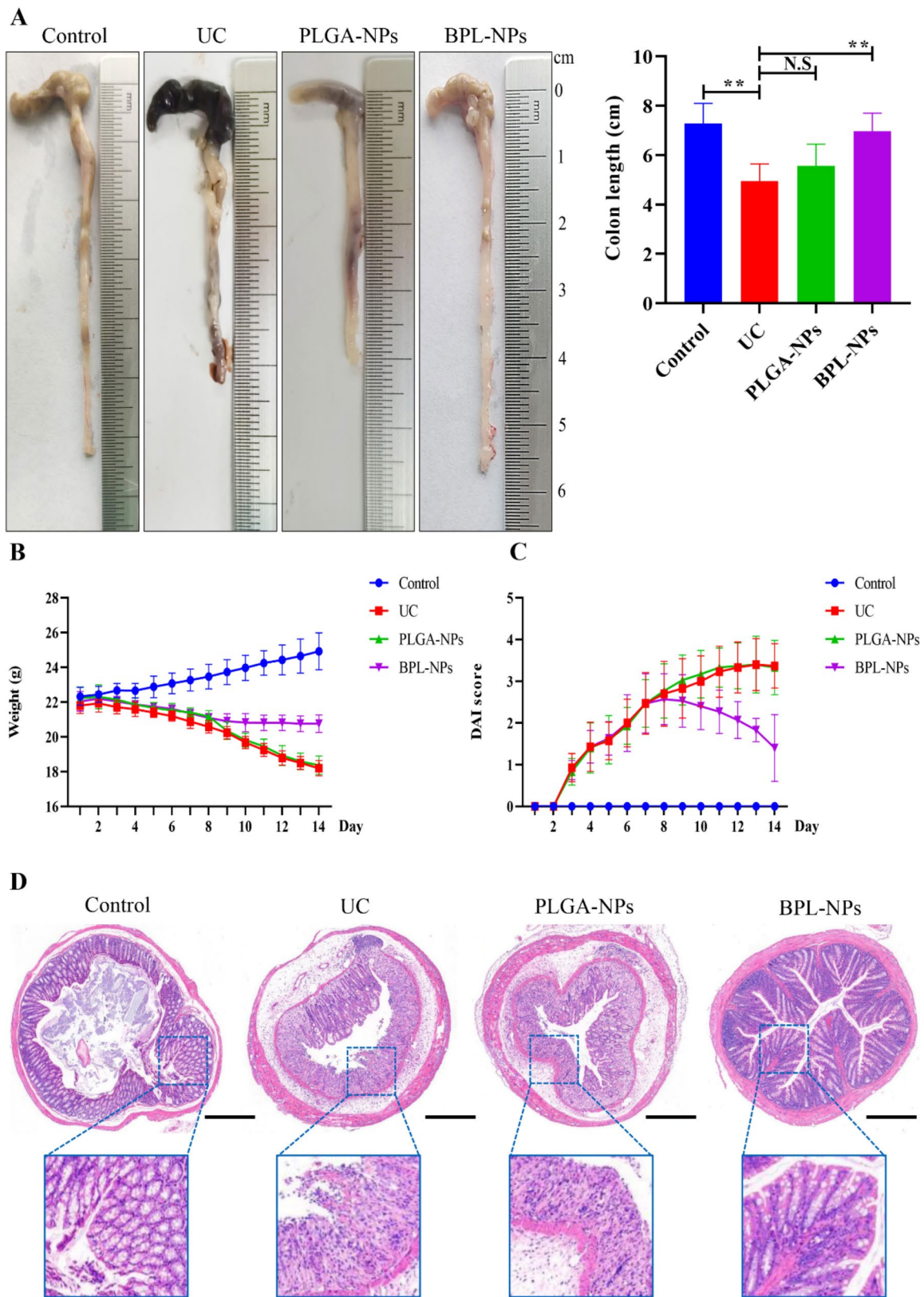


Fig. 4 Effects of BPL-NPs treatment on UC mice. **A:** A colon length measurement was performed on mice ($n=10$) in each group, $**P<0.01$ versus UC group, N.S.: None statistically significant; **B:** Body weight of mice ($n=10$) in each group; **C:** DAI values of mice ($n=10$) in each group; **D:** H&E staining of individual mice groups. Scale bars = 200 μ m

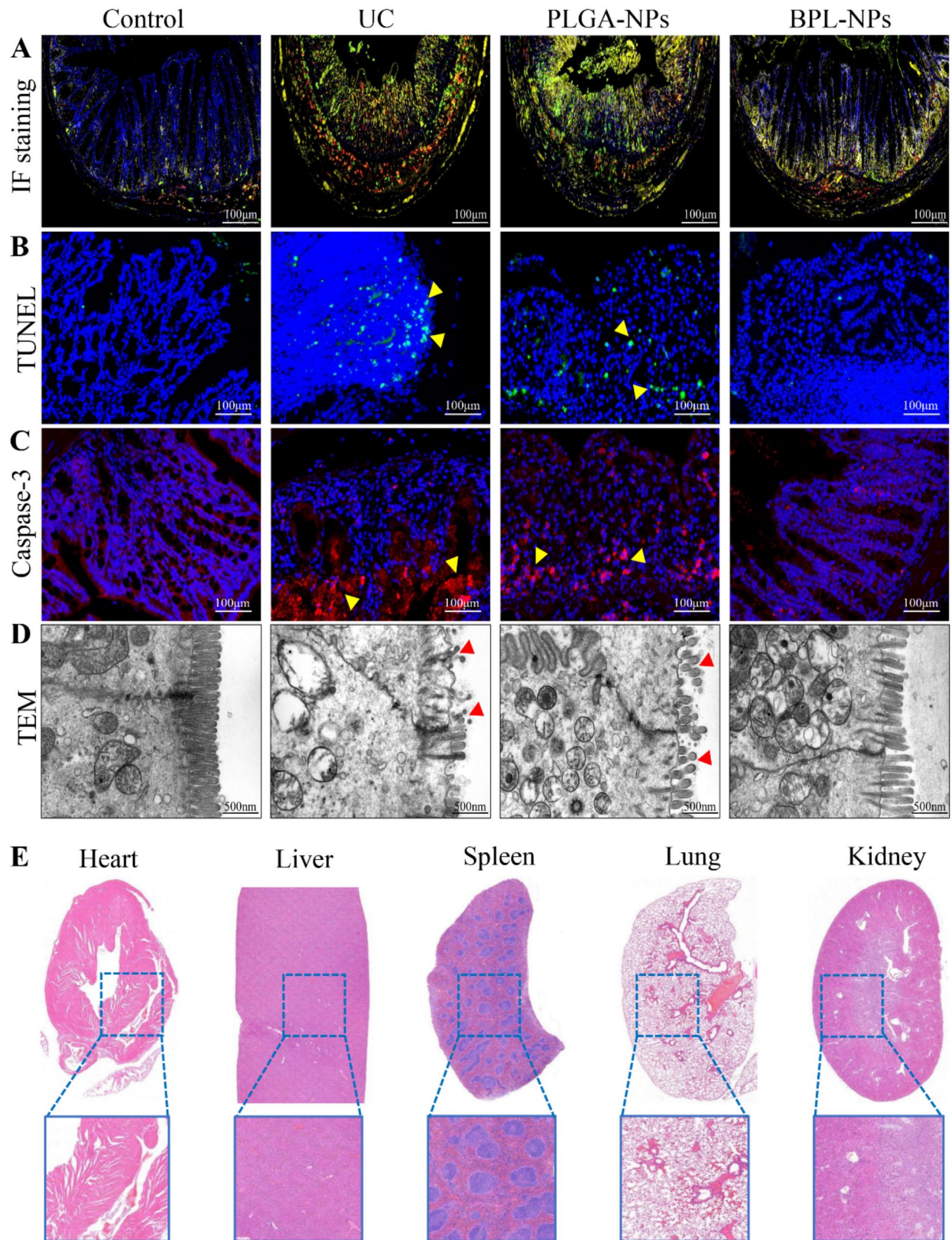


Fig. 5 BPL-NPs on the apoptosis of IECs and mucosal barrier function. **A**: IF staining of F4/80⁺ (red fluorescence), CD86⁺ (green fluorescence), IL6⁺ (yellow fluorescence) in each group of mice; **B**: TUNEL staining of colonic sections in each group of mice; **C**: IF staining of Caspase-3 in each group of mice; **D**: Microstructure of colonic epithelia observed using TEM; **E**: Results of HE staining

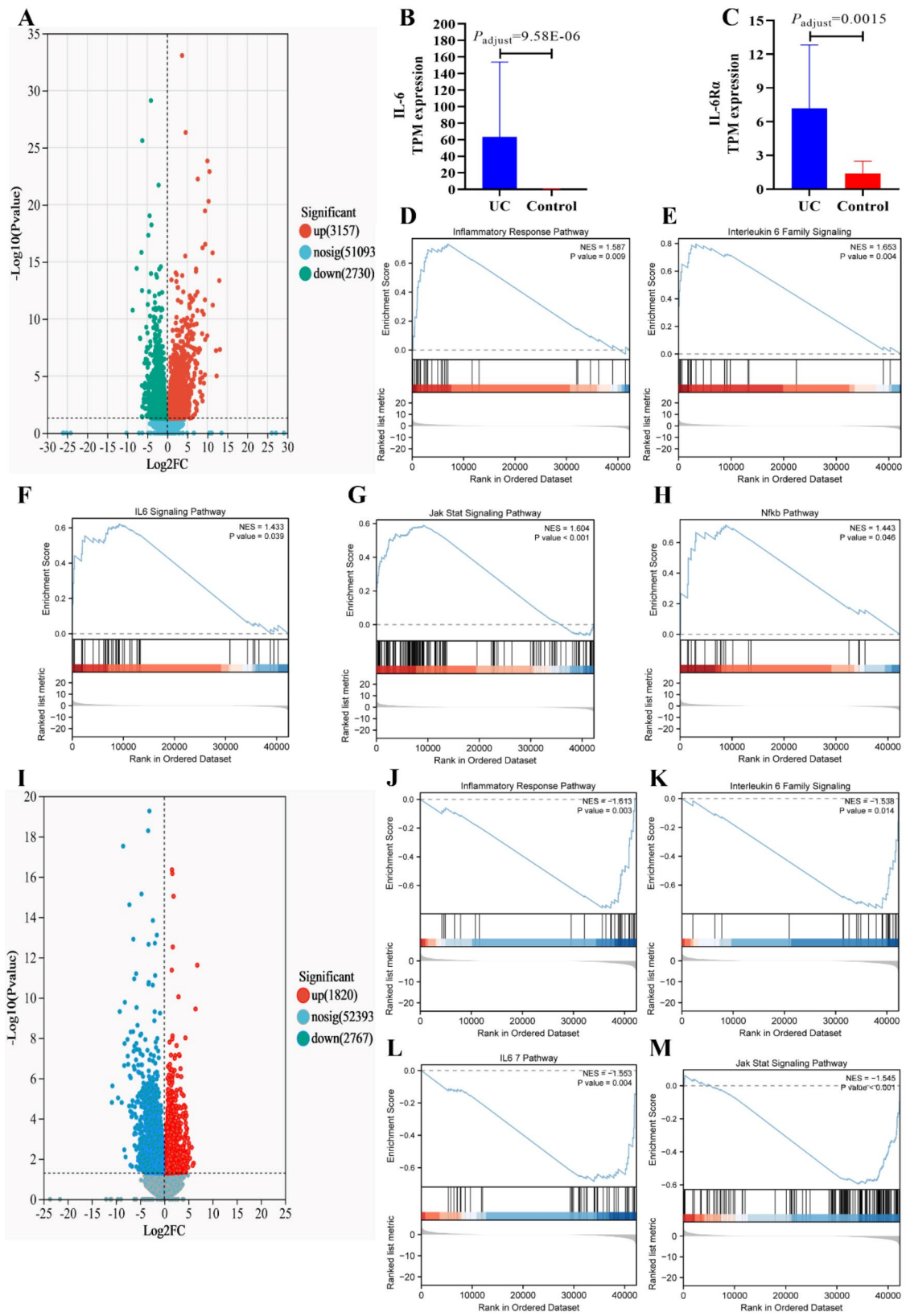


Fig. 6 (See legend on next page.)

(See figure on previous page.)

Fig. 6 Results of the transcriptomics analysis and GSEA between groups ($n=5$). **A:** Volcano plot of DEGs between UC and control groups; **B:** TPM expression of Il-6 between UC and control groups; **C:** GSEA of inflammatory response pathway between UC and control groups; **D:** GSEA of Il-6R α between UC and control groups; **E:** GSEA of interleukin 6 family signaling between UC and control groups; **F:** GSEA of Il-6 signaling pathway between UC and control groups; **G:** GSEA of Jak/Stat signaling pathway between UC and control groups; **H:** GSEA of Nf- κ b Pathway between UC and control groups; **I:** Volcano plot of DEGs between BPL-NPs and UC groups; **J:** GSEA of inflammatory response pathway between BPL-NPs and UC groups; **K:** GSEA of interleukin 6 family signaling between BPL-NPs and UC groups; **L:** GSEA of Il-6/7 pathway between BPL-NPs and UC groups; **M:** GSEA of Jak/Stat signaling pathway between BPL-NPs and UC groups

Jak/Stat signaling pathway (Fig. 6G), and Nf- κ b Pathway (Fig. 6H), were also significantly upregulated in the UC phenotype, which was consistent with the findings reported in previous studies (Fig. 3B and C). In contrast, the transcriptional expression in the UC mice underwent a change in the opposite direction due to the intervention of BPL-NPs. As presented in Fig. 6I and Table S8, 4587 DEGs were detected in the BPL-NPs vs. UC groups, of which 1820 were upregulated and 2767 were down-regulated. In addition, the phenotype of the BPL-NPs group showed significant down-regulation of various inflammatory pathways, such as the inflammatory response pathway (Fig. 6J, Table S9), interleukin 6 family signaling (Fig. 6K), Il6/7 pathway (Fig. 6L), and Jak/Stat signaling pathway (Fig. 6M). Thus, based on these results, it was hypothesized that BPL-NPs primarily affect the phenotype of the inflammatory response, with the inhibitory process possibly involving the Il-6 and Jak/Stat signaling pathways.

BPL-NPs inhibited Il-6/Stat3 signaling pathway in UC mice

The transcriptomics analysis revealed that BPL-NPs significantly inhibited the expression of Il6 and the Jak/Stat signaling pathway in mice with UC. Accordingly, additional research into the molecular mechanism at the mRNA level and PCR array analysis was conducted. The mRNA expression heat map revealed a significant down-regulation of most genes associated with the activators, receptors, and targets of the Il-6/Stat3 signaling pathway after treatment with BPL-NPs (Fig. 7A, Table S10). Furthermore, the expression of activator genes (Il-6 and Cxcl12, Fig. 7B and C), receptor genes (Il6 α and Il6st, Fig. 7D and E), downstream signaling genes (Bax and Stat3, Fig. 7F and G), and target genes (Ccl12 and Sosc3, Fig. 7H and I) in the Il-6/Stat3 signaling pathway were also significantly down-regulated following treatment with BPL-NPs. Accordingly, it was hypothesized that the down-regulation of upstream or downstream genes in the Il-6/Stat3 signaling pathway played a pivotal role in the therapeutic effects of BPL-NPs in the treatment of UC.

BPL-NPs inhibited IL-6/IL-6R axis to ameliorate apoptosis of NCM-460 cells

To clarify the molecular targeting of BPL-NPs, *in vitro* verification experiments were conducted. Previous studies have demonstrated that a higher ratio of M1 M ϕ s

significantly promotes proinflammatory responses and triggers apoptosis of IECs in UC [28, 29]. Accordingly, the impact of M1 M ϕ s on NCM-460 cells was evaluated in the current study. As shown in Fig. 8A, following a 6-hour stimulation by LPS, M1 M ϕ s exhibited a significantly higher production of IL-6 than M0 M ϕ s. Furthermore, the highest level of IL-6 was observed at the 12-hour mark. The protein expression of IL-6 was consistently and significantly increased in M1 M ϕ s, as shown in Fig. 8B. Subsequently, a co-cultivation system (Fig. 8C) was used to investigate the impact of M1 M ϕ s on NCM-460 cells. Following a 24-hour co-culture with M1 macrophages, the apoptosis of NCM-460 cells was significantly increased (Fig. 8D). Based on the findings, it was hypothesized that the apoptosis of NCM-460 cells could be associated with the increased secretion of IL-6 by M1 M ϕ s. In addition, the IL-6R membrane receptor of NCM-460 cells, rather than gp130 (as shown in Fig. 8E), was found to be dominantly activated by the elevated levels of IL-6 produced by M1 M ϕ s. Subsequently, the expression of IL-6R was suppressed in NCM-460 cells, which were then co-cultured with M1 M ϕ s. As a result, in comparison to the siNC group, there were significantly fewer apoptotic cells (Fig. 8F and G). Conversely, the BPL-NPs group exhibited a decrease in apoptotic cells, as evidenced by Fig. 8F and G. This reduction was similar to the effects observed in the siIL-6R groups. These results suggest that BPL-NPs specifically targeted the IL-6/IL-6R axis to induce apoptosis in NCM460 cells stimulated by M1 M ϕ s.

BPL-NPs targeted the IL-6/IL-6R axis to suppress the downstream signaling pathway

To gain a deeper understanding of how BPL-NPs specifically target the IL-6/IL-6R axis at a molecular level, the downstream signaling expression of the IL-6/IL-6R axis was evaluated in the current study. BPL-NPs effectively suppressed the Jak/Stat signaling pathway, the Nf- κ b pathway (Fig. 6), and the Il-6/Stat3 signaling pathway (Fig. 7) in UC mice, as confirmed by the previous findings. Consequently, the JAK/STAT3 and NF- κ B pathway were verified, following the inhibition of the IL-6/IL-6R axis. As shown in Fig. 9A and S6, the presence of BPL-NPs significantly reduced the expression of IL-6R in NCM-460 cells when co-cultivated with M1 M ϕ s. Consistently, the protein expression of IL-6 and IL-6R was also significantly down-regulated by the BPL-NPs

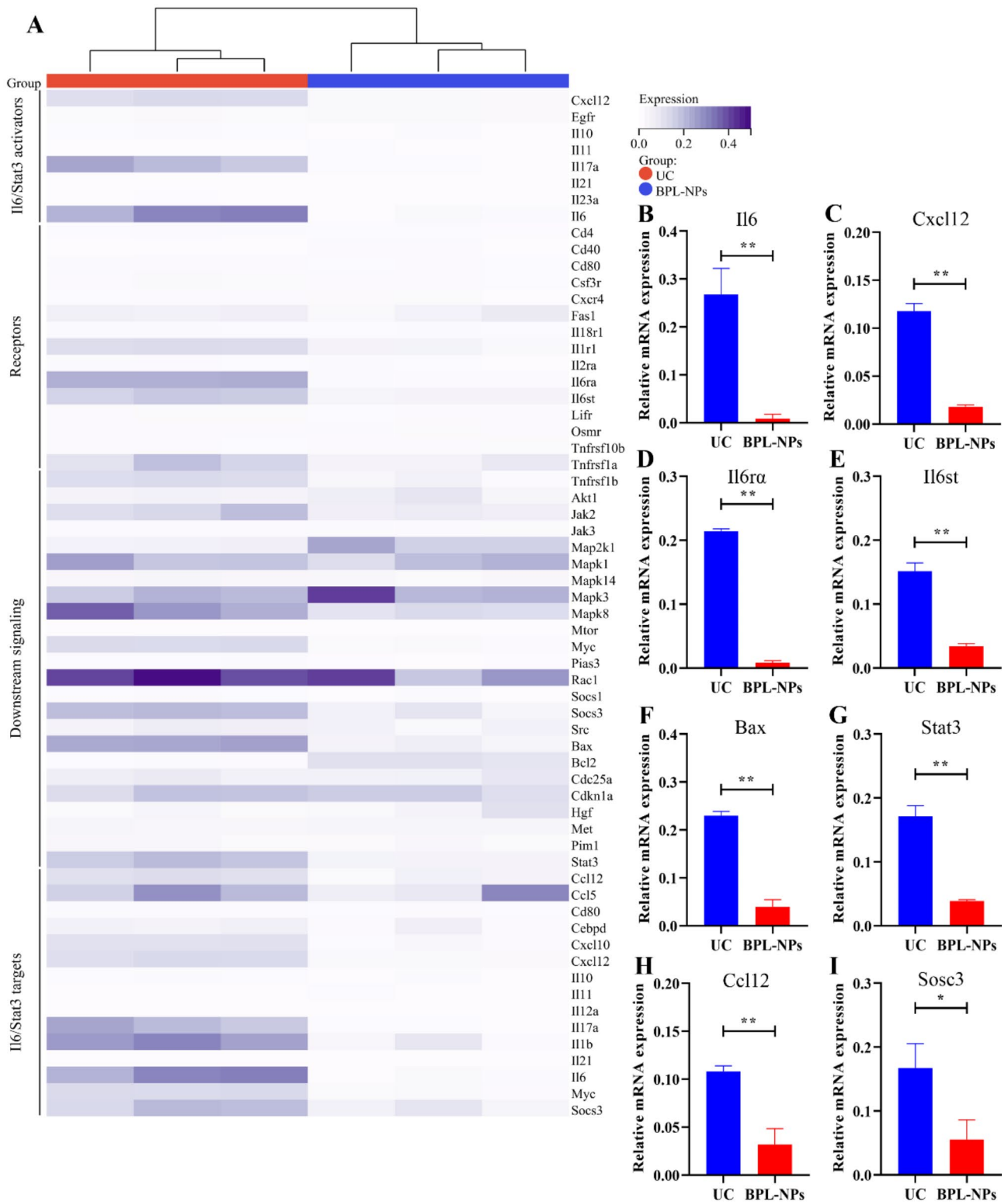


Fig. 7 Gene expression of the Il-6/Stat3 signaling pathway in the UC and BPL-NPs groups (n=3). **A**: Heat map of relative mRNA expression; **B, C**: mRNA expression of Il-6 and Cxcl12; **D, E**: mRNA expression of Il6ra and Il6st; **F, G**: mRNA expression of Bax and Stat3; **H, I**: mRNA expression of Ccl12 and Sosc3. * $P < 0.05$, ** $P < 0.01$

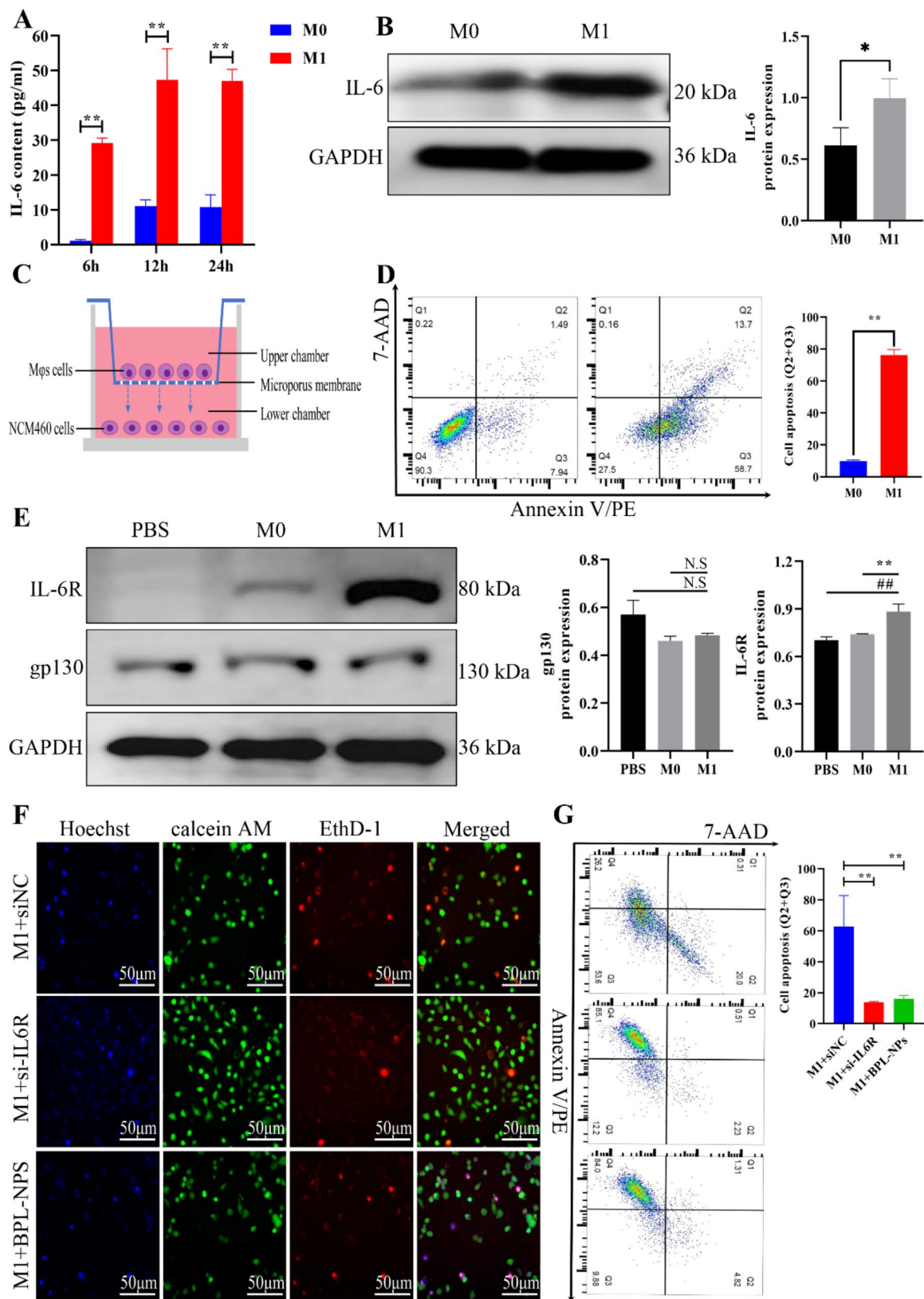


Fig. 8 Effects of BPL-NPs on the apoptosis of NCM-460 cells induced by M1 Mφs. A: IL-6 content in cell supernatant detected by ELISA, ** $P < 0.01$; B: Protein expression of IL-6, * $P < 0.05$; C: Schematic diagram of the co-cultivation system; D: Apoptosis rate of the NCM-460 cells, as detected by FCM, ** $P < 0.01$; E: Protein expression of IL-6R and gp130, ** $P < 0.01$ versus M0 group, ** $P < 0.01$ versus PBS group, N.S.: None statistically significant; F: HCS images of NCM-460 cells co-cultured with M1 Mφs; G: Apoptotic cell count of NCM-460 among different groups, ** $P < 0.01$

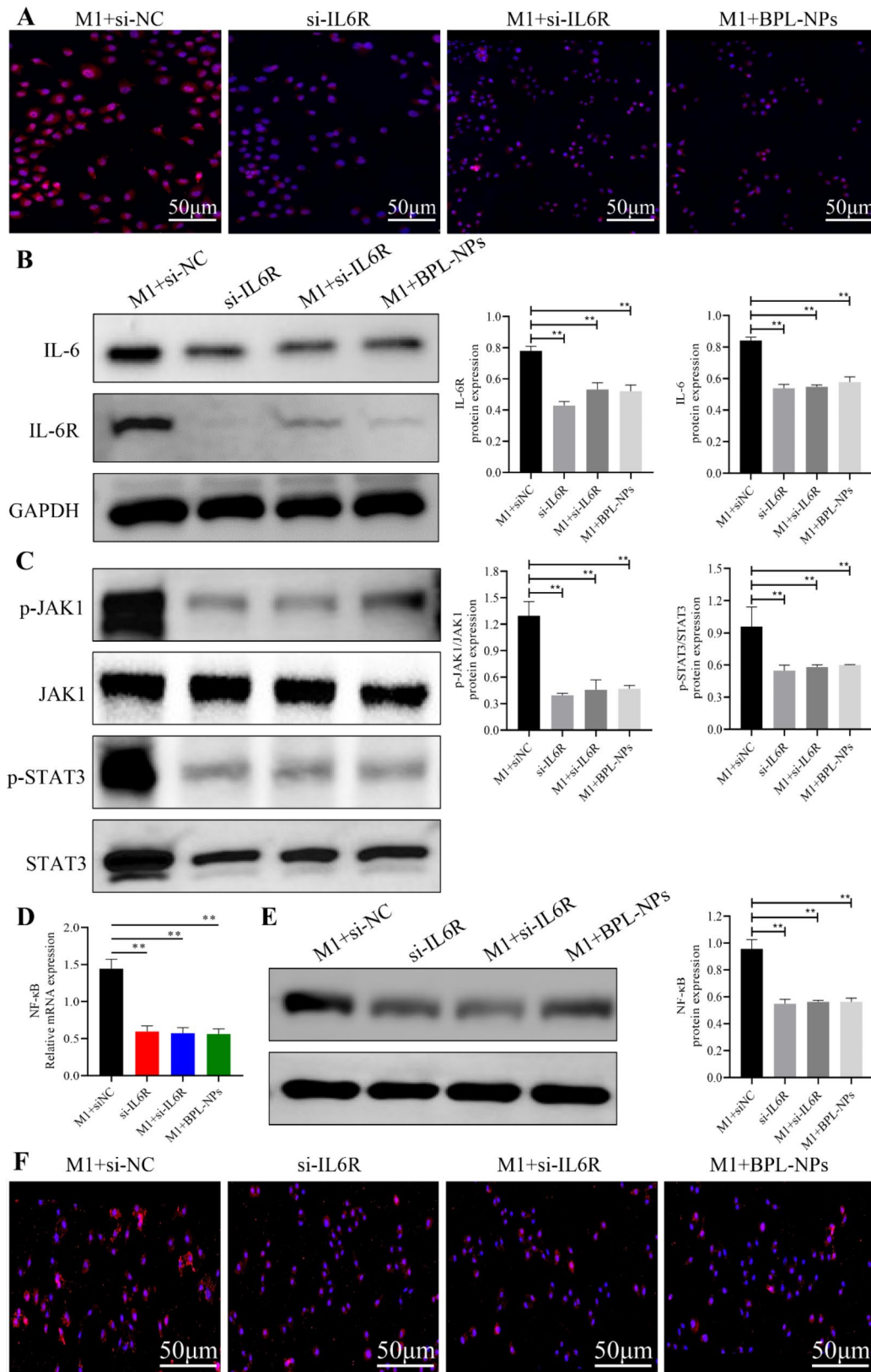


Fig. 9 Targeting of IL-6/IL-6R axis by BPL-NPs and the associated downstream signals. A: IF staining of IL-6R in NCM-460 cells; B: Protein expression of IL-6 and IL-6R; C: Total protein expression and phosphorylation level of JAK1, STAT3, p-JAK1, and p-STAT3; D: Relative mRNA expression of NF-κB; E: Protein expression of NF-κB; F: IF staining of Caspase-3 in NCM-460 cells. ****** $P < 0.01$

(Fig. 9B). Thus, after validating that the IL-6/IL-6R axis was being targeted for inhibition, the downstream signals of the axis, such as JAK/STAT3 and NF- κ B were evaluated. As presented in Fig. 9C, the phosphorylation level of p-JAK1 and p-STAT3 was significantly down-regulated by BPL-NPs. Furthermore, the mRNA (Fig. 9D) and protein expression (Fig. 9E) of NF- κ B were markedly down-regulated by BPL-NPs. As observed, following the inhibition of IL-6/IL-6R axis-related signals, the intervention of BPL-NPs primarily resulted in a decrease in the marker of activated apoptosis, Caspase-3 (Fig. 9F, Fig. S7). Correspondingly, these results demonstrate that BPL-NPs specifically targeted and inhibited the IL-6/IL-6R axis and its downstream signals.

Discussion

The development of safe and safe drug delivery systems targeting the affected tissue area is an urgent need for the effective treatment of UC. The retention enema has been shown to result in higher levels of drug in target tissues while minimizing systemic side effects in the treatment of UC [30]. Compared to the systemic administration of therapeutics through intravenous injection, targeted drugs delivered via retention enema enable direct drug enrichment to the colitis tissues. This reduces the occurrence of systemic adverse drug reactions, while concomitantly increasing the concentration of drugs in the target tissue. In spite of this, local-acting medications often suffer from poor intrarectal retention time when administered with enemas, resulting in urgent defecation, which reduces their therapeutic effectiveness. It is also uncomfortable to have to administer enemas repeatedly to achieve the necessary therapeutic dosage [31]. Thus, delivery systems rapidly absorbed by the inflamed colonic tissue following intrarectal infusion in patients with UC and offer longer residence time are urgently needed. In the present study, BBR-encapsulated PLGA NPs (BPL-NPs) were fabricated using emulsion solvent-driven self-assembly. Specific molecular weight of PLGA was selected for the purpose of conducting our experiment. Dichloromethane was employed as a solvent due to its low water solubility, low boiling point, and high solubility in organic compounds. Finally, various doses of berberine were combined with PLGA to formulate nanoparticles. The optimal ratio of berberine to PLGA was determined by assessing the particle size and dispersion index of the resultant nanoparticles. By meticulously controlling these parameters, uniform nanoparticles were produced, thereby enhancing their therapeutic efficacy. To mitigate the impact of residual dichloromethane on the release behavior of nanoparticles, we initially optimized the quantity of dichloromethane utilized during the preparation process. Subsequently, dichloromethane was removed using a rotary evaporator, followed by dialysis

in deionized water and freeze-drying. These measures collectively ensure a significant reduction in the adverse effects of residual dichloromethane on the release behavior of nanoparticles, thereby enhancing their efficacy and safety in practical applications. The findings demonstrated that the BPL-NPs were rapidly absorbed by the cell membrane/cytoplasm of IECs and could prolong the residence time of BBR in the inflamed colonic tissue. Furthermore, using an enema mode of administration theoretically increased the accumulated concentration of BPL-NPs in the inflamed colon, while offering no apparent toxicity to the vital organs.

The significant pathological changes associated with UC are typically characterized by an immune-mediated inflammatory disorder of the colon and rectum, resulting in mucosal damage and apoptosis of IECs. In particular, the pathogenesis of UC is characterized by a complex inflammatory environment consisting of innate and adaptive immune cells that infiltrate the lamina propria. M ϕ s, which comprise a subset of leukocytes and an essential part of the innate immune system, are essential to maintaining intestinal homeostasis. Accordingly, the classical (M1-like phenotype) and alternative (M2-like phenotype) activation of M ϕ s have been extensively studied and understood. In the context of UC, an increasing amount of evidence has identified that M1-like M ϕ s exacerbate UC via the disorderly release of a wide range of proinflammatory cytokines, including IL-6, IL-1 β , and tumor necrosis factor- α (TNF- α). The pro-inflammatory cytokines facilitate the transmission of messages within cells by interacting with intracellular proteins, such as Janus kinases (JAK), which further potentiate the activation and proliferation of lymphocytes in the affected intestinal region [32]. Previous studies have also confirmed that M1-like M ϕ s in UC patients were significantly concentrated in the inflamed region of the colon [33]. In addition, the increased presence of M1 M ϕ s in the immune system, along with elevated levels of pro-inflammatory cytokines in the mucous membranes of the colon and rectum, further aggravate the inflammation of the intestinal lining and apoptosis of IECs [34]. In this study patients with UC had a higher presence of M1 M ϕ s in their intestinal mucosa. This suggests that targeting these M ϕ s could serve as a potential therapeutic approach for effectively managing UC. In this context, previous studies [11, 35, 36] have demonstrated that inhibiting M1 M ϕ s and their cytokines in UC mice effectively contributed to the treatment of UC. In addition, the use of PLGA-based NPs that were capable of specifically targeting M1 M ϕ s in UC significantly improved the therapeutic efficacy [37, 38]. Furthermore, BPL-NPs not only improved the water solubility of BBR in this study but also inhibited the infiltration of M1 M ϕ s infiltration, leading to improved therapeutic outcomes in UC. These

findings, therefore, suggest that BPL-NPs can serve as a novel therapeutic approach for UC with high targeting efficacy and minimal systemic toxicity.

Very few novel studies suggest that targeting M1 M ϕ s or their pro-inflammatory cytokines/pathways can effectively ameliorate UC. Interleukin-6 (IL-6) is a pro-inflammatory cytokine that M1 M ϕ s secrete. The biological effects of IL6 are mediated through two primary mechanisms: classic signaling, which occurs when IL6 binds to its membrane-bound IL6 receptor (IL-6R α), and trans-signaling, which arises when IL6 binds to a soluble form of IL6R (s-IL6R) and then to the membrane-bound transducer glycoprotein 130 (gp130) [39]. Classic signaling via membrane receptor (IL-6R α) has been identified to contribute to developing inflammatory bowel diseases (IBD). Accordingly, pharmacological inhibitors of IL-6 signaling were developed to prevent IL-6 from binding to IL-6R by targeting either IL-6 or the receptors. Previous studies have demonstrated that the complete inhibition of IL-6 activity, achieved by blocking the receptor or the cytokine using monoclonal antibodies, could be a potential option for targeted biological therapy in IBD [40]. In this context, tocilizumab, an anti-IL-6R monoclonal antibody first used in 2004 in a phase I clinical trial, has been recognized as a promising therapeutic option in managing IBD in numerous studies [41, 42]. Nevertheless, a study conducted by Atreya et al., [43] demonstrated that the administration of tocilizumab resulted in increased mucosal ulcers and inflammation in patients with UC. The failure of tocilizumab is likely caused by the additional impairment of epithelial barrier integrity, which subsequently leads to the activation of mucosal immune cells resulting in the production of pro-inflammatory cytokines (such as TNF, IFN- γ , or IL-21) and progressive ulcer formation [44]. Given that IL-6 signaling plays a role in both the progression of IBD and the repair of the mucosal lining, optimizing therapeutic inhibitors that target the IL-6/IL-6R signaling pathway during the stages of inflammation where IL-6 production is dysregulated offers significant promise [45]. In addition, the selective induction of IL-6 during the stage of mucosal healing could be a useful approach to treating IBD [45]. In the present study, the IL-6 signaling pathway was observed to be over-activated, leading to increased immune infiltration of M1 M ϕ s in UC. Accordingly, the classic signaling pathway mediated by the membrane receptor IL-6R α , rather than the trans-signaling pathway involving s-IL6R, was predominantly activated by IL-6 derived from the M1 M ϕ s. Furthermore, BPL-NPs were found to specifically target the IL-6/IL-6R axis both in vitro and in vivo, without impairing the integrity of the epithelial barrier or worsening inflammation or apoptosis. Consequently, the therapeutic effect of BPL-NPs is ascribed to the inhibition of the IL-6/IL-6R axis.

There is no denying that this current study has some limitations. Firstly, there is a gap between DSS-induced UC model and human UC due to differences in species, genome, living environment, psychology and food intake. The incidence of UC is the result of the long-term effects of social and individual, physiological and psychological factors. DSS-induced UC model only simulates the clinical manifestations of UC, but cannot completely present the whole process of UC disease. Secondly, this study paid more attention to the short-term efficacy of BPL-NPs and did not evaluate long-term efficacy and safety, which resulted in it only being applied as preclinical research. The treatment effects and safety of BPL-NPs need to be further validated in human clinical trials. Finally, the internal feedback mechanisms between biological signaling pathways and molecules are quite complex, which contributes to the off-target effects of BPL-NPs.

In conclusion, an anti-inflammatory nano-delivery system based on BBR and PLGA-based NPs was developed in this current study to enhance their bioactivity and water solubility for use in the treatment of UC. Compared to free BBR, the improved therapeutic effects of BPL-NPs were accompanied by reduced particle size, increased capsulation efficiency, water solubility, and bioactivity. The in vitro and in vivo selective targeting of the IL-6/IL-6R axis was confirmed as the mechanism by which BPL-NPs induced the therapeutic effects in UC. In addition, the potential modality of BPL-NPs in treating UC or another immune inflammatory disease (such as Crohn's disease) could involve enema administration to bypass first-pass elimination effects, leading to increased local concentration. Oral administration should also be explored.

Supplementary Information

The online version contains supplementary material available at <https://doi.org/10.1186/s12967-024-05682-x>.

Supplementary Material 1
Supplementary Material 2
Supplementary Material 3
Supplementary Material 4
Supplementary Material 5
Supplementary Material 6
Supplementary Material 7
Supplementary Material 8
Supplementary Material 9
Supplementary Material 10
Supplementary Material 11
Supplementary Material 12
Supplementary Material 13
Supplementary Material 14

Supplementary Material 15

Supplementary Material 16

Supplementary Material 17

Acknowledgements

The financial support of this study is the National Natural Science Foundation of China (No. 82260936), NATCM's Project of High-level Construction of Key TCM Disciplines (No. zyyzdxk-2023188), Guizhou Science and Technology Project (No. Basic-ZK[2024] General 399). We thank all the reviewers who participated in the review work.

Author contributions

Xinhao Yan, Tao Yang: funding acquisition, methodology, project administration, supervision, validation, visualization, writing original draft, and writing–review & editing. Chao Liu and Qiming Gong: methodology, software, visualization, writing–original draft, and writing–review & editing. Wanning Liu and Yihan Zhao: formal analysis, methodology, software, visualization.

Data availability

All data generated or analyzed during this study are included in this published article and supplementary material.

Declarations

Conflict of interest

All authors of this manuscript state that they do not have any conflict of interest, and there is nothing to disclose.

Author details

¹Cardiovascular Medicine Department, Xijing Hospital, Fourth Military Medical University, Xi'an 710032, China

²Department of Nephrology, Affiliated Hospital of Youjiang Medical University for Nationalities, No.18 Zhongshan Road, Guangxi, China

³Baise Key Laboratory for Metabolic Diseases, Youjiang Medical University for Nationalities), Education Department of Guangxi Zhuang Autonomous Region, Baise 533000, China

⁴College of Life Sciences, Northwest University, Xi'an 710069, China

⁵Second Clinical College, Shanxi University of Traditional Chinese Medicine, Xi'an 712046, China

⁶Key Laboratory of Clinical Molecular Biology, Hanzhong Vocational and Technical College, No.81, West side of National Road 316, Hanzhong 723002, China

⁷State Key Laboratory of Holistic Integrative Management of Gastrointestinal Cancers, Xijing Hospital of Digestive Diseases, Fourth Military Medical University, No. 127, Changle West Road, Xi'an 710032, China

⁸Colorectal and Anal Surgery, the First Affiliated Hospital of Guizhou University of Traditional Chinese Medicine, No. 71 Baoshan North Road, Guiyang 550001, China

Received: 6 July 2024 / Accepted: 9 September 2024

Published online: 24 October 2024

References

- Du L, Ha C. Epidemiology and Pathogenesis of Ulcerative Colitis. *Gastroenterol Clin North Am.* 2020;49(4):643–54.
- Ben-Horin S, Har-Noy O, Katsanos KH, Roblin X, Chen M, Gao X, et al. Corticosteroids and Mesalamine Versus corticosteroids for Acute severe Ulcerative Colitis: a Randomized Controlled Trial. *Clin Gastroenterol Hepatol.* 2022;20(12):2868–e751.
- Manzini R, Schwarzfischer M, Atrott K, Laimbacher A, Lang S, Sawrzyniak M, et al. Combination of Vedolizumab with Tacrolimus is more efficient Than Vedolizumab alone in the treatment of experimental colitis. *Inflamm Bowel Dis.* 2021;27(12):1986–98.
- Nakase H, Uchino M, Shinzaki S, Matsuura M, Matsuoka K, Kobayashi T, et al. Evidence-based clinical practice guidelines for inflammatory bowel disease 2020. *J Gastroenterol.* 2021;56(6):489–526.
- Sadeghi N, Mansoori A, Shayesteh A, Hashemi SJ. The effect of curcumin supplementation on clinical outcomes and inflammatory markers in patients with ulcerative colitis. *Phytother Res.* 2020;34(5):1123–33.
- Xu X, Zhang J, Chen L, Sun Y, Qing D, Xin X, et al. Alhagi pseudalhagi Extract exerts protective effects against intestinal inflammation in Ulcerative Colitis by affecting TLR(4)-Dependent NF- κ B signaling pathways. *Front Pharmacol.* 2021;12:764602.
- Gowd V, Kanika, Jori C, Chaudhary AA, Rudayni HA, Rashid S, et al. Resveratrol and resveratrol nano-delivery systems in the treatment of inflammatory bowel disease. *J Nutr Biochem.* 2022;109:109101.
- Deng SP, Yang YL, Cheng XX, Li WR, Cai JY. Synthesis, Spectroscopic Study and Radical Scavenging Activity of Kaempferol Derivatives: enhanced water solubility and antioxidant activity. *Int J Mol Sci.* 2019;20(4).
- Gao C, Liu L, Zhou Y, Bian Z, Wang S, Wang Y. Novel drug delivery systems of Chinese medicine for the treatment of inflammatory bowel disease. *Chin Med.* 2019;14:23.
- Singh NK, Dhanasekaran M, Kumar AHS. Pharmacology of Berberine and its metabolites, is it the nature's ozempic or Imatinib? *Arch Pharmacol Ther.* 2023;5(1):67–81.
- Xiong K, Deng J, Yue T, Hu W, Zeng X, Yang T, et al. Berberine promotes M2 macrophage polarisation through the IL-4-STAT6 signalling pathway in ulcerative colitis treatment. *Heliyon.* 2023;9(3):e14176.
- Yang T, Ma X, Wang R, Liu H, Wei S, Jing M, et al. Berberine inhibits IFN- γ signaling pathway in DSS-induced ulcerative colitis. *Saudi Pharm J.* 2022;30(6):764–78.
- Yang T, Qin N, Liu F, Zhao Y, Liu W, Fan D. Berberine regulates intestinal microbiome and metabolism homeostasis to treat ulcerative colitis. *Life Sci.* 2024;122385.
- Prosperi D, Colombo M, Zanoni I, Granucci F. Drug nanocarriers to treat autoimmunity and chronic inflammatory diseases. *Semin Immunol.* 2017;34:61–7.
- Ahmad A, Ansari MM, Mishra RK, Kumar A, Vyawahare A, Verma RK, et al. Enteric-coated gelatin nanoparticles mediated oral delivery of 5-aminosalicylic acid alleviates severity of DSS-induced ulcerative colitis. *Mater Sci Eng C Mater Biol Appl.* 2021;119:111582.
- Ahmad A, Ansari MM, Kumar A, Bishnoi M, Raza SS, Khan R. Aminocellulose-grafted polycaprolactone-coated core-shell nanoparticles alleviate the severity of ulcerative colitis: a novel adjuvant therapeutic approach. *Biomater Sci.* 2021;9(17):5868–83.
- Jin M, Li S, Wu Y, Li D, Han Y. Construction of Chitosan/Alginate Nano-Drug Delivery System for improving Dextran Sulfate-Induced Colitis in mice. *Nanomaterials (Basel).* 2021;11(8).
- Xu Y, Huang J, Fan Y, Long H, Liang M, Chen Q, et al. Macrophage-targeted berberine-loaded β -Glucan nanoparticles enhance the treatment of Ulcerative Colitis. *Int J Nanomed.* 2022;17:5303–14.
- Rampado R, Caliceti P, Agostini M. Latest advances in Biomimetic Cell membrane-coated and membrane-derived nanovectors for Biomedical Applications. *Nanomaterials (Basel).* 2022;12(9).
- Ding D, Zhu Q. Recent advances of PLGA micro/nanoparticles for the delivery of biomacromolecular therapeutics. *Mater Sci Eng C Mater Biol Appl.* 2018;92:1041–60.
- Zhu K, Yao Y, Wang K, Shao F, Zhu Z, Song Y, et al. Berberin sustained-release nanoparticles were enriched in infarcted rat myocardium and resolved inflammation. *J Nanobiotechnol.* 2023;21(1):33.
- Comincini S, Manai F, Sorrenti M, Perteghella S, D'Amato C, Miele D et al. Development of Berberine-Loaded Nanoparticles for Astrocytoma Cells Administration and photodynamic therapy stimulation. *Pharmaceutics.* 2023;15(4).
- Wirtz S, Popp V, Kindermann M, Gerlach K, Weigmann B, Fichtner-Feigl S, et al. Chemically induced mouse models of acute and chronic intestinal inflammation. *Nat Protoc.* 2017;12(7):1295–309.
- Im K, Mareninov S, Diaz MFP, Yong WH. An introduction to performing immunofluorescence staining. *Methods Mol Biol.* 2019;1897:299–311.
- Yang T, Wang R, Zhang J, Bao C, Zhang J, Li R, et al. Mechanism of berberine in treating *Helicobacter pylori* induced chronic atrophic gastritis through IRF8-IFN- γ signaling axis suppressing. *Life Sci.* 2020;248:117456.
- Li K, Strauss R, Ouahed J, Chan D, Telesco SE, Shouval DS, et al. Molecular Comparison of Adult and Pediatric Ulcerative Colitis Indicates Broad Similarity of Molecular Pathways in Disease tissue. *J Pediatr Gastroenterol Nutr.* 2018;67(1):45–52.

27. Wang H, Yuan M, Wang S, Zhang L, Zhang R, Zou X et al. STAT3 regulates the type I IFN-Mediated antiviral response by interfering with the Nuclear entry of STAT1. *Int J Mol Sci.* 2019;20(19).
28. Wu MM, Wang QM, Huang BY, Mai CT, Wang CL, Wang TT, et al. Dioscin ameliorates murine ulcerative colitis by regulating macrophage polarization. *Pharmacol Res.* 2021;172:105796.
29. Zhang Q, Chen LH, Yang H, Fang YC, Wang SW, Wang M, et al. GPR84 signaling promotes intestinal mucosal inflammation via enhancing NLRP3 inflammasome activation in macrophages. *Acta Pharmacol Sin.* 2022;43(8):2042–54.
30. Kumar A, Kanika, Kumar V, Ahmad A, Mishra RK, Nadeem A, et al. Colon-adhering delivery system with inflammation responsiveness for localized therapy of experimental colitis. *ACS Biomater Sci Eng.* 2023;9(8):4781–93.
31. Ingram JR, Rhodes J, Evans BK, Newcombe RG, Thomas GA. Comparative study of enema retention and preference in ulcerative colitis. *Postgrad Med J.* 2005;81(959):594–8.
32. Horn F, Henze C, Heidrich K. Interleukin-6 signal transduction and lymphocyte function. *Immunobiology.* 2000;202(2):151–67.
33. Qiu P, Liu L, Fang J, Zhang M, Wang H, Peng Y, et al. Identification of pharmacological Autophagy regulators of active Ulcerative Colitis. *Front Pharmacol.* 2021;12:769718.
34. Wang J, Wu Z, Huang Y, Jin L, Xu J, Yao Z et al. IRF4 induces M1 macrophage polarization and aggravates ulcerative colitis progression by the Bcl6-dependent STAT3 pathway. *Environ Toxicol.* 2024.
35. Lv Q, Xing Y, Liu Y, Chen Q, Xu J, Hu L, et al. Didymin switches M1-like toward M2-like macrophage to ameliorate ulcerative colitis via fatty acid oxidation. *Pharmacol Res.* 2021;169:105613.
36. Zhuang H, Lv Q, Zhong C, Cui Y, He L, Zhang C, et al. Tiliroside ameliorates Ulcerative Colitis by restoring the M1/M2 macrophage balance via the HIF-1 α /glycolysis pathway. *Front Immunol.* 2021;12:649463.
37. Zhou Y, Yang M, Yan X, Zhang L, Lu N, Ma Y, et al. Oral nanotherapeutics of Andrographolide/Carbon Monoxide Donor for synergistically anti-inflammatory and pro-resolving treatment of Ulcerative Colitis. *ACS Appl Mater Interfaces.* 2023;15(30):36061–75.
38. Li Z, Zhang X, Liu C, Peng Q, Wu Y, Wen Y, et al. Macrophage-biomimetic nanoparticles ameliorate Ulcerative Colitis through reducing inflammatory factors expression. *J Innate Immun.* 2022;14(4):380–92.
39. Parisinos CA, Serghiou S, Katsoulis M, George MJ, Patel RS, Hemingway H, et al. Variation in interleukin 6 receptor Gene associates with risk of Crohn's Disease and Ulcerative Colitis. *Gastroenterology.* 2018;155(2):303–e62.
40. Schreiber S, Aden K, Bernardes JP, Conrad C, Tran F, Höper H, et al. Therapeutic Interleukin-6 trans-signaling inhibition by Olamkicept (sgp130Fc) in patients with active inflammatory bowel disease. *Gastroenterology.* 2021;160(7):2354–e6611.
41. Ito H. Treatment of Crohn's disease with anti-IL-6 receptor antibody. *J Gastroenterol.* 2005;40(Suppl 16):32–4.
42. Szeto MC, Yalçın MD, Khan A, Piotrowicz A. Successful use of Tocilizumab in a patient with Coexisting Rheumatoid Arthritis and Ulcerative Colitis. *Case Rep Immunol.* 2016;2016:7562123.
43. Atreya R, Billmeier U, Rath T, Mudter J, Vieth M, Neumann H, et al. First case report of exacerbated ulcerative colitis after anti-interleukin-6R salvage therapy. *World J Gastroenterol.* 2015;21(45):12963–9.
44. Shahini A, Shahini A. Role of interleukin-6-mediated inflammation in the pathogenesis of inflammatory bowel disease: focus on the available therapeutic approaches and gut microbiome. *J Cell Commun Signal.* 2023;17(1):55–74.
45. Choi JS, Kim KH, Lau LF. The matricellular protein CCN1 promotes mucosal healing in murine colitis through IL-6. *Mucosal Immunol.* 2015;8(6):1285–96.

Publisher's note

Springer Nature remains neutral with regard to jurisdictional claims in published maps and institutional affiliations.